Bioactive Materials 24 (2023) 497–506

Contents lists available at ScienceDirect

Bioactive Materials

journal homepage: www.keaipublishing.com/en/journals/bioactive-materials

Potential Alzheimer's disease therapeutic nano-platform: Discovery of amyloid-beta plaque disaggregating agent and brain-targeted delivery system using porous silicon nanoparticles

Jaehoon Kim [a,1], Hyeji Um [a,1], Na Hee Kim [a], Dokyoung Kim [a,b,c,d,e,f,*]

[a] Department of Biomedical Science, Graduate School, Kyung Hee University, Seoul, 02447, Republic of Korea
[b] Medical Research Center for Bioreaction to Reactive Oxygen Species and Biomedical Science Institute, Kyung Hee University, Seoul, 02447, Republic of Korea
[c] Department of Anatomy and Neurobiology, College of Medicine, Kyung Hee University, Seoul, 02447, Republic of Korea
[d] Center for Converging Humanities, Kyung Hee University, Seoul, 02447, Republic of Korea
[e] KHU-KIST Department of Converging Science and Technology, Kyung Hee University, Seoul, 02447, Republic of Korea
[f] UC San Diego Materials Research Science and Engineering Center, 9500 Gilman Drive La Jolla, CA, 92093, USA

ARTICLE INFO

Keywords:
Alzheimer's disease
Plaques disaggregation
Nanotherapeutics
Brain-targeted drug delivery
Porous silicon nanoparticles

ABSTRACT

There has been a lot of basic and clinical research on Alzheimer's disease (AD) over the last 100 years, but its mechanisms and treatments have not been fully clarified. Despite some controversies, the amyloid-beta hypothesis is one of the most widely accepted causes of AD. In this study, we disclose a new amyloid-beta plaque disaggregating agent and an AD brain-targeted delivery system using porous silicon nanoparticles (pSiNPs) as a therapeutic nano-platform to overcome AD. We hypothesized that the negatively charged sulfonic acid functional group could disaggregate plaques and construct a chemical library. As a result of the in vitro assay of amyloid plaques and library screening, we confirmed that 6-amino-2-naphthalenesulfonic acid (ANA) showed the highest efficacy for plaque disaggregation as a hit compound. To confirm the targeted delivery of ANA to the AD brain, a nano-platform was created using porous silicon nanoparticles (pSiNPs) with ANA loaded into the pore of pSiNPs and biotin-polyethylene glycol (PEG) surface functionalization. The resulting nano-formulation, named Biotin-CaCl2-ANA-pSiNPs (BCAP), delivered a large amount of ANA to the AD brain and ameliorated memory impairment of the AD mouse model through the disaggregation of amyloid plaques in the brain. This study presents a new bioactive small molecule for amyloid plaque disaggregation and its promising therapeutic nano-platform for AD brain-targeted delivery.

1. Introduction

As the number of the elderly population increases, the incidents of degenerative brain diseases such as Alzheimer's disease (AD), Parkinson's disease, and Huntington's disease are also on the rise [1–4]. Since the first report of AD in 1906, numerous studies have been conducted in the research fields of pathogenesis, lesions, symptoms, and treatments [5–9]. Despite tremendous efforts to understand AD, its exact causes and treatment have yet to be clearly identified [10,11]. The amyloid hypothesis is one of the widely accepted causes of AD [12–14]. Amyloid-beta (Aβ) monomers, which can be present in any body part including the brain, can form Aβ plaque that causes severe toxicity in the AD patient's brain [15,16]. Currently, several therapeutic methods are available based on the Aβ hypothesis, such as the β-secretase enzyme (BACE1) inhibitor and anti-Aβ antibody development [17–19]. However, the objective should be to remove Aβ plaques from the brain, and therefore it is crucial to find new molecules for Aβ plaque disaggregation and its delivery system to the AD brain [20,21].

In this study, we disclose a therapeutic nano-platform for Aβ plaque disaggregating in an AD brain (Fig. 1a). The Aβ plaque disaggregating nano-platform (APDN) consists of an Aβ disaggregating agent, an agent-delivery nano-carrier, and an AD brain targeting moiety. Among the various nano-carriers, porous silicon nanoparticles (pSiNPs) were selected as an ideal APDN for their advantages of high biocompatibility,

Peer review under responsibility of KeAi Communications Co., Ltd.
* Corresponding author. Department of Biomedical Science, Graduate School, Kyung Hee University, Seoul, 02447, Republic of Korea.
E-mail address: dkim@khu.ac.kr (D. Kim).
[1] These authors contributed equally.

https://doi.org/10.1016/j.bioactmat.2023.01.006
Received 3 October 2022; Received in revised form 4 December 2022; Accepted 5 January 2023

high drug-loading efficiency, and facile surface modification [22–24]. Next, we select biotin as a brain-targeting moiety among several known moieties, including transferrin, lectin, ApoE, glutathione, biotin, and so on, because it has known to exist in abundance in the brain, especially in the hippocampus, which is most closely related to AD and memory [25–30]. Therefore, we hypothesized that more drugs could be delivered to the hippocampus region by surface modification using biotin. The APDN can penetrate the blood-brain barrier (BBB) and be accumulated via biotin receptor binding and endocytosis through the endothelial cells [31–33]. Our research rationale is based on the two steps (Fig. 1b). (1) Step 1: In vitro Aβ plaque disaggregation screening. Several previous studies have shown that sulfonic acid could bind to and disaggregate amyloid beta plaques [34–38]. Referring to the existing studies on Aβ plaque disaggregating agents, we hypothesized that the negatively charged sulfonic acid functional group could disaggregate Aβ plaques. In this study, a new agent library was constructed in order to confirm the difference in Aβ plaque disaggregation efficacy according to the case where functional groups other than the previously known hydroxy group or piperazine group were combined with sulfonic acid as a base or according to the length of the carbon branch to which sulfonic acid was linked to other functional groups. The agent library (number of chemicals >20) was constructed containing various substances, including sulfonic acid and similar structural analogs, to find a hit compound tracking the disaggregation level of Aβ plaques after treatment of the agent library via thioflavin T (ThT) assay. (2) Step 2: Nano-carrier loading on the hit compound and surface functionalization. Typically, negatively charged molecules have limitations in BBB penetration, and so does our hit compound for practical applications [39,40]. To address such a delivery issue, a nano-carrier was introduced to efficiently deliver the hit compound to the AD brain. The final nano-formulation was demonstrated to improve memory impairment through an animal behavioral experiment of the Aβ plaque-injected AD mouse model. In addition, changes in interleukin 6 (IL-6) level, which is known to be increased by Aβ plaques [41,42], and the amount of Aβ plaques in the hippocampus were also measured through Thioflavin S (ThS) staining [43].

We found a new Aβ plaque disaggregating agent and constructed its therapeutic nano-platform. In the animal experiment, the APDN-treated AD mice showed significant memory retention with a reduced number of Aβ plaques in the brain. We believe that our findings can open new doors in AD treatment and a new era in AD-related basic research and clinical applications.

2. Experimental section

2.1. Amyloid beta (1-42) plaques preparation

Amyloid-beta (Aβ) 1–42 (Anaspec, AS-20276, MW = 4514.1, 1 mg) was dissolved in 1 × PBS buffer (pH 7.4, 1 mL) to a final concentration of 222 μM. This solution was incubated (200 rpm) for 3 days at 37 °C and used for in vitro experiments without further purification [44]. The formed Aβ plaques were confirmed by the thioflavin T (ThT) assay (Fig. S1).

2.2. Hit compound identification

As-prepared Aβ plaques (10 μM) were stirred (200 rpm) at 37 °C for 24 h in the presence of the screening candidates (100 μM) within PBS (pH 7.4). Then, thioflavin T (ThT, 10 μM) was added to confirm the plaque disaggregation results. A: 4-(2-Hydroxyethyl)-1-piperazinepropanesulfonic acid (EPPS); B: 2-[4-(2-hydroxyethyl)piperazin-1-yl]ethanesulfonic acid (HEPES); C: sulfamic acid; D: aminomethanesulfonic acid; E: 2-aminoethanesulfonic acid; F: 2-aminoethanesulfonic acid; G: sulfuric acid; H: 3-hydroxypropanesulfonic acid; I: benzenesulfonic acid; J: 4-hydroxybenzenesulfonic acid; K: sulfanilic acid; L: 3-amino-4-hydroxybenzenesulfonic acid; M: naphthalene; N: 2-naphthalenesulfonic acid; O: 2-naphthol-6-sulfonic acid; P: 6-amino-2-naphthalenesulfonic acid (ANA); Q: 4-amino-1-naphthalenesulfonic acid; R: 5-amino-1-naphthalenesulfonic acid; S: 6-amino-4-hydroxy-2-naphthalenesulfonic acid; T: 6-amino-1-naphthol-3-sulfonic acid. Absorption and emission spectra of ThT were obtained using UV/vis absorption spectroscopy (Agilent, California, USA) and spectrofluorophotometer (Shimadzu Corp., Kyoto, Japan).

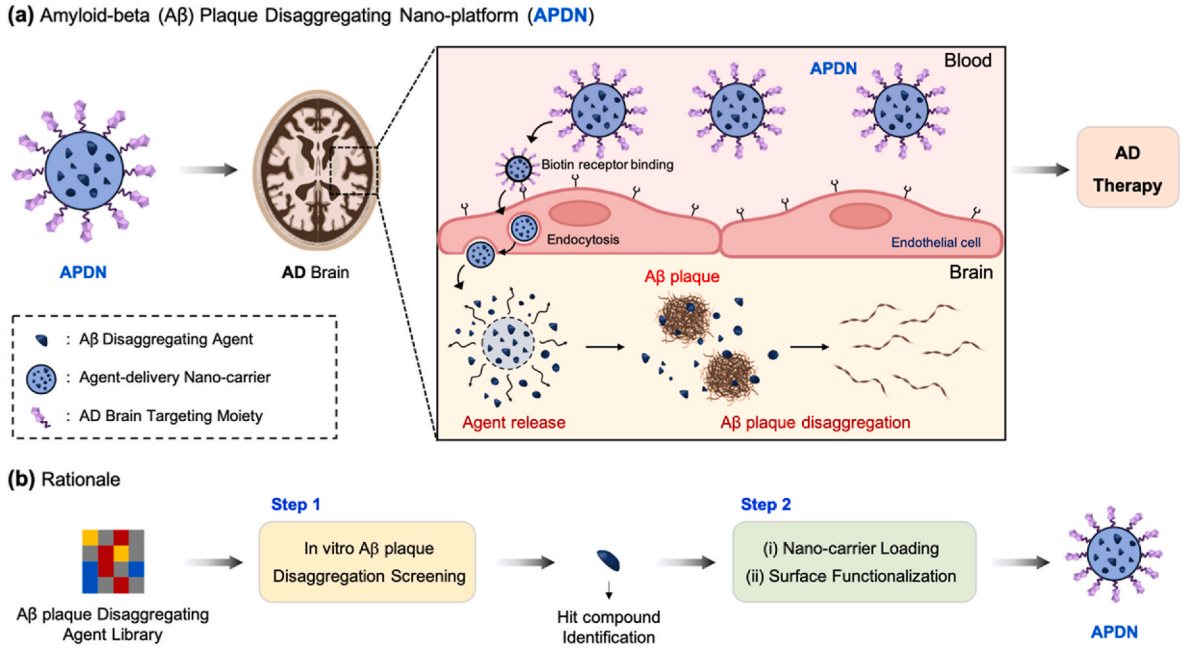

Fig. 1. (a) Schematic illustration of amyloid-beta (Aβ) plaque disaggregating nano-platform (APDN). (b) Research rationale. Step 1: a hit compound discovery via in vitro Aβ plaque disaggregation screening using the Aβ disaggregating agent library. Step 2: Nano-carrier loading on the hit compound derived from Step 1, and surface functionalization for Alzheimer's disease (AD) brain targeting.

2.3. Transmission electron microscopy (TEM) imaging

Samples for TEM analysis were prepared using the following method [45]; (i) A copper grid was treated with samples (5 μL) from either Aβ plaques (10 μM) or Aβ plaque disaggregation form at room temperature. The excessive samples on the grids were removed by washing three times with DI H_2O. (ii) Each grid was stained with uranyl acetate (1% w/v DI H_2O, 5 μL) for 1 min. Uranyl acetate was blotted off, and the grids were dried for 20 min at room temperature. (iii) The morphology of samples was analyzed by transmission electron microscopy (TEM, Tecnai, G2 F30ST, FEI Company, OR, USA) imaging at Korea Basic Science Center (Korea University, Seoul, Rep. of Korea).

2.4. Thioflavin S (ThS) assay

The presence of Aβ plaques and amyloid-beta plaque disaggregation form (incubated with the screening candidates for 24 h) were also assessed by thioflavin S (ThS)-based fluorescence analysis [43]. The samples (Aβ plaques, Aβ plaques with screening candidates) were added to 1 mL of ThS (0.5%) solution. The mixture was pipetted onto the slide-glass and dried at room temperature overnight. Then, fluorescence images were obtained using a laser scanning confocal microscope (CLSM, LSM800, Zeiss, Oberkochen, Germany). The confocal images were obtained under excitation at 520 nm (Laser power: 3.00%) with a detector (GaAsP, Detector gain: 680 V; Detector wavelength: 548–617 nm).

2.5. Preparation of porous silicon nanoparticles (pSiNPs)

The pSiNPs were prepared by electrochemical etching of p^{++}-type single-crystal silicon wafers (highly boron-doped); (i) A silicon wafer was electrochemically etched in an electrolyte (48% aqueous HF/absolute ethanol (EtOH), 3:1, v: v). [Caution: HF is highly toxic, and proper care should be exerted to avoid contact with skin or lungs]. (ii) Before preparing the porous silicon (pSi) layer, the silicon wafer was electrochemically etched on a porous sacrificial layer with 3:1 (v:v) 48% aqueous HF/ethanol electrolyte. (iii) The resulting pSi layer was removed using 2 M potassium hydroxide solution (KOH). The perforated etching waveform was applied: a lower current density pulse of 46 mA cm^{-2} for 1.8 s and a higher current density pulse of 334 mA cm^{-2} for 0.4 s, repeated for 300 cycles. The porous Si film was then detached from the silicon wafer by applying a current density pulse of 3 mA cm^{-2} for 300 s in a solution of 7.5% aqueous HF in ethanol (lift-off step). (iv) The free-standing pSi film was placed in a sealed glass vial (22.18 mL size, VWR, Product No. 66011-143, Radnor, PA, USA) containing deionized water (DI H_2O, 6 mL) and fractured to nanoparticles in an ultrasonic bath (VWR, Model No. VWRA142-0307, Radnor, PA, USA) for 24 h. (v) After sonication, the porous silicon nanoparticles (pSiNPs) were further incubated in DI H_2O (12 mL) for 3 days at 25 °C to form a silicon oxide layer on the surface, and then filtered through a 0.22 μm syringe filter (Millipore, Millex syringe filter unit, 220 nm, Model No. SLGP033RS, Burlington, MA, USA). (vi) The filtered pSiNPs were collected by centrifugation (14000 rpm, 15 min) and redispersed/washed with EtOH (3 times).

2.6. Preparation of Biotin-$CaCl_2$-ANA-pSiNPs (BCAP)

ANA stock solution (10 mg/mL DMSO, 100 μL) was added to the solution of pSiNPs (1 mg) dispersed in DI H_2O (400 μL). The mixture was reacted with the 4 M $CaCl_2$ stock solution (500 μL) for 2 h using a vortex mixer (600 rpm, Scientific industries, Inc., VortexGenie 2, Model No. SI-0246, Bohemia, NY, USA) at room temperature. The $CaCl_2$-ANA-pSiNPs (CAP) were collected by centrifugation (14000 rpm, 15 min) and washed with DI H_2O (1 mL) three times. Then, silane-PEG-biotin (5000 Da) stock solution (100 μL, 10 mg/mL, EtOH) was added to the solution of CAP dispersed in EtOH (900 μL) and mixed using a vortex mixer for 2 h at room temperature. After 2 h, the resulting BCAP was washed using EtOH (1 mL) three times and collected by centrifugation (14000 rpm, 15 min)

2.7. Characterization of nanoparticles

To identify the structural changes of the pSiNPs nano-formulations, the hydrodynamic size, zeta-potential, and infrared absorption spectrum of the pSiNPs nano-formulations were analyzed using Malvern Instruments Zetasizer Nano and Attenuated total reflection Fourier transform infrared (ATR-FTIR) spectroscopy. In order to observe the structural changes of each formulation, image-based analysis was conducted by transmission electron microscopy (TEM).

2.8. Release profiling of BCAP

The release profile of the loaded ANA from BCAP was measured by tracking the fluorescence signals of ANA using a spectrofluorophotometer (Shimadzu Corp. RF-6000, Kyoto, Japan). BCAP (1 mg) was dispersed in PBS (1 mL, pH 7.4), and the solution was incubated at 37 °C for the time intervals (0–120 min). At each time interval (30 min, 60 min, 90 min, and 120 min), BCAP was removed from the aqueous phase by centrifugation at 14000 rpm for 15 min. The supernatant was analyzed to determine the amount of the released ANA from BCAP using a 1-cm standard quartz cell (internal volume of 1 mL, Hellma Analytics, Germany).

2.9. Animals

Six-week-old male balb/c mice were obtained from DBL Co., Ltd. (Incheon, Rep. of Korea). Each cage housed 5 mice (27 × 22 × 14 cm) that had free access to food and water in the animal room under a 12-h light/dark cycle (lights on from 07:30–19:30) at a constant temperature (23 ± 1 °C) and relative humidity (60 ± 10%). The mice stayed in the animal room for a week before the experiments. Animal treatment and maintenance were performed according to the Animal Care and Use Guidelines by Kyung Hee University. All experimental protocols were approved by the Institutional Animal Care and Use Committee of Kyung Hee University (Approval number: KHSASP-22-024).

2.10. Tissue imaging

After the BCAP (10 mg/kg, i.v.) administration and circulation (2 h), the mice were anesthetized and transcardially perfused with PBS (pH 7.4) and fixed with 4% paraformaldehyde. The main organs (brain, heart, lung, spleen, kidney, and liver) were dissected to perform further ex vivo analysis. The fluorescence tissue imaging system (FTIS, VISQUE® InVivo Elite, Vieworks Co. Ltd., Rep. of Korea) was used for ex vivo tissue fluorescence imaging. The imaging experiment was carried out in a dark room. The data were acquired by tracking the signals of ANA (Channel: 390–490 nm excitation, 500–550 nm detection channel).

2.11. Hemolysis test

The blood was obtained from the hearts of the mice anesthetized with isofluorane. The red blood cells (RBCs) were extracted by centrifugation at 4 °C (3,000 rpm, 3 min) and washed in 1 × cold PBS (2 times). The concentrations (ANA or BCAP) for the test were 0.03, 0.1, 0.3, 1, and 3 mg/mL. ANA or BCAP were treated to the purified RBCs (8% working concentration, v/v, in cold 1 × PBS). [Positive control: 0.1% (working concentration) Triton X-100]. The mixture was incubated in a shaking incubator (200 rpm, 37 °C) for 1 h and then was centrifuged at 3000 rpm at 4 °C. The supernatant was measured under absorption at 450 nm.

2.12. Mouse model

The prepared amyloid-beta plaque (222 μM) was stereotaxically administered (1 μL/min for 5 min) to bregma of the mice under anesthesia of isoflurane via intracerebroventricular (i.c.v.) injection using a Hamilton microsyringe (−0.2 mm anteroposterior (AP), −1 mm mediolateral (ML), and −2.4 mm dorsoventral (DV)) [46]. The stereotaxic surgical procedure was performed in a separate heated room whose heating system controls the body temperature of the mice (maintained at 36–37 °C). The temperature was monitored regularly using a thermometer as the body temperature drop during anesthesia can induce tau phosphorylation.

2.13. Y-maze test

The Y-maze is constructed with three dark opaque polyvinyl plastic arms (40 × 3 × 12 cm) positioned at a 120-degree angle from each other [47]. The last administration of PBS, ANA, CAP, and BCAP was 1 h before the test. The sham group received a vehicle solution instead of ANA. Each mouse was initially placed in one arm, and the sequence of arm entry (i.e., ABC, CAB, etc.) was recorded over 8 min using a video camera-based EthoVision System (Noldus, Netherlands). Between each test, a 70% EtOH spray was used to remove any residual odors and residues in the Y-maze arms. An actual alternation was defined as an entry into all three arms consecutively (i.e., ABC, BAC, or CAB but not BCC or CCA). The actual alternation was manually observed by a person who was unaware of to the treatment. The alternation score (%) for each mouse was defined as the ratio of the number of actual alternations to the possible number of alternations (defined as the total number of arm entries minus two) multiplied by 100, as indicated in the following equation: % alternation = [(number of alternations)/(total arm entry numbers–2)] × 100.

2.14. Passive avoidance test (PAT)

The PAT has been used to measure long-term memory in mice. The passive avoidance test was performed over two consecutive days for an acquisition and retention trial in an apparatus consisting of two attached chambers (20 × 20 × 20 cm) connected by a door (5 × 5 cm) [48]. One chamber was a light chamber (50 W bulb) and the other was a dark chamber without a light source. Both chamber floors have 2 mm stainless steel bars at 1 cm intervals. On the first day, the acquisition trial was conducted. The mice were put gently in the light chamber. The door between the light chamber and dark chamber was opened 10 s later and was closed automatically after the mice entered the dark chamber. Then, an electrical shock (0.5 mA, 3 s) was applied to the mice's foot through the stainless-steel bars. If a mouse did not enter the dark chamber within 60 s, it was forced to enter the dark chamber, and the latency was recorded as 60 s. The retention trial was performed 24 h after the acquisition trial. The mice were put in the light chamber, and the door was opened 10 s later, under the same condition as the acquisition trial. The time taken for the mice to enter the dark chamber was recorded, and the mice were not given an electric shock this time. The maximum latency was set up to 300 s. If a mouse did not enter the dark chamber after the door was opened, the latency was recorded as 300 s.

2.15. ELISA assay

The blood collected from the mouse model was centrifuged for 3 min at 3,000 rpm and 4 °C and the plasma (supernatant) was collected for protein analysis. Interleukin 6 (IL-6) in the plasma of the mouse models was measured using an ELISA kit (Novex, Model No. KMC0061, US), following the manufacturer's protocol.

2.16. ThS tissue staining

The mice were sacrificed after the passive avoidance test and were subjected to perfusion with PBS (50 mM, pH 7.4) and fixation (4% paraformaldehyde). After perfusion, brains were removed with post-fixation overnight at 4 °C and incubated in 30% sucrose at 4 °C. Sequential 25-μm-thick coronal sections were prepared by a cryostat (CM1850; Leica, Wetzlar, Germany) and stored at 4 °C. Free-floating sections were incubated for 10 min in 1% thioflavin S dissolved in 50% ethanol, followed by two washes with 50% ethanol for 5 min, respectively, and one wash with distilled water for 5 min; the sections were then stained by applying mounting medium.

2.17. Statistical analysis

The data are presented as the mean ± standard error of the mean (S.E.M). The ThS intensity was analyzed by unpaired t-tests. The results of the IVIS data, hemolysis test, Y-maze test, PAT, and ELISA assay were analyzed by one-way analysis of variance (ANOVA) with Tukey's multiple comparison test. All statistical results were analyzed by Prism 8.0 software (GraphPad, La Jolla, CA, USA).

3. Results and discussion

3.1. Library screening and hit compound identification

First, the Aβ plaque disaggregating agent library containing sulfonic acid and similar structures (Fig. 2a) was constructed as aliphatic sulfonic acid compounds including EPPS and HEPES are reported to have Aβ plaque disaggregation properties, which was addressed in our previous work. However, such compounds require high concentration for AD therapeutic applications, and their low brain-targeting with BBB penetration is considered a critical weakness. To address such issues, we tried to find a new agent from the sulfonic acid-containing molecular library. The library consists of simple aliphatic sulfonic acid analogs (A–H), benzene sulfonic acid analogs (I–L), and naphthalene sulfonic acid analogs (M–T). The hydroxyl group and primary amine group were introduced to verify the hydrogen-bonding effect of analogs toward Aβ plaques, and the aromatic rings were introduced to verify the hydrophobicity and lipophilicity effect.

A hit compound from the library was identified by thioflavin T (ThT) assay (Fig. 2b). ThT could bind to Aβ plaques and has a fluorescence turn-on signal. The candidates (from the agent library, 100 μM) were treated to the complex of Aβ plaque (10 μM) and ThT (10 μM), and the fluorescence signal changes were monitored after incubating for 24 h at 37 °C. After 24 h, UV/vis absorption and emission spectra changes of ThT were measured (Fig. 2c, Fig. S1, Fig. S2). The emission intensity of compounds at 482 nm, which is the maximum peak of ThT, confirmed that compound P, 6-amino-2-naphthalenesulfonic acid (ANA), exhibited 23.11% of the original emission intensity where only Aβ plaques existed, and its intensity change was the most significant. Similar results were verified by other known Aβ plaque sensing dyes, including Nile red and AOI 987 (Fig. S3). Under the given experimental condition, compounds A (EPPS) and B (HEPES) showed no significant activity for Aβ plaque disaggregation. The only difference between ANA and the compound O/Q-R is the functional group and the location of sulfonic acid, but their Aβ plaque disaggregating ability significantly differs. Our study focuses on identifying the property of ANA and its therapeutic ability. To understand the working concentration of ANA, ANA (0–100 μM) was treated with a mixed solution of Aβ plaques (10 μM) and dye (10 μM) and incubated for 24 h at 37 °C. Then, UV/vis absorption and emission spectra of dye were measured (Fig. 2d, Fig. S3). The results confirmed that ANA can be efficacious even at concentrations as low as 10 and 30 μM, which is an enormous advantage in drug development. Next, the Aβ plaque disaggregating ability of ANA was measured at various pHs (3, 5, 7, 7.4, and 9) to see if there was a change in the efficacy according to the

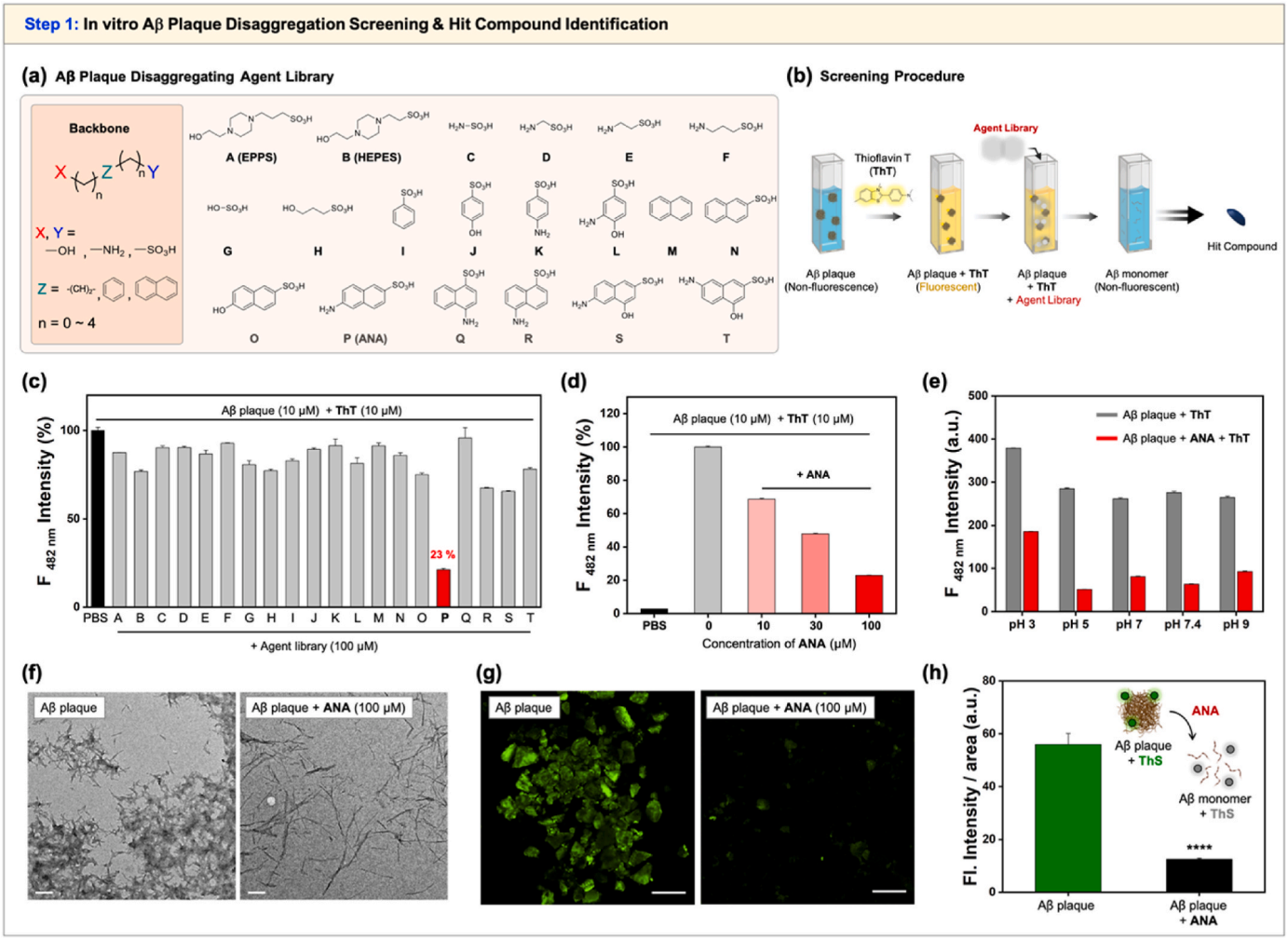

Fig. 2. (a) Aβ plaque disaggregating agent library. (b) In vitro Aβ plaque disaggregation screening procedure using thioflavin T (ThT) assay to identify a hit compound from the Aβ disaggregating agent library. (c) The emission intensity plot (at 482 nm) of ThT (10 μM) in the presence of Aβ plaque (10 μM) and the agent library (100 μM) in PBS buffer (pH 7.4) at 25 °C. Excitation wavelength: 413 nm. Incubation time: 24 h. The data are shown as the means ± S.E.M. (n = 3). (d) The emission intensity plot (at 482 nm) of ThT (10 μM) in the presence of Aβ plaque (10 μM) and ANA (10–100 μM) in PBS buffer (pH 7.4) at 25 °C. Excitation wavelength: 413 nm. Incubation time: 24 h. The data are shown as the means ± S.E.M. (n = 3). (e) The emission intensity plot (at 482 nm) of ThT (10 μM) in the presence of Aβ plaque (10 μM) and ANA (100 μM) in various pH buffers at 25 °C. Excitation wavelength: 413 nm. Incubation time: 24 h. The data are shown as the means ± S.E.M. (n = 3). (f) Transmission electron microscope (TEM) images and (g) confocal images of Aβ plaques (20 μM) with/without ANA (100 μM) treatment. Scale bar: 200 nm. Excitation and emission channel: 520 nm, 548–617 nm. (h) The emission intensity plots of Aβ plaques (20 μM) with/without ANA (100 μM) from confocal images. The data are shown as the means ± S.E.M. (n = 8). ****<0.0001 when compared to the non-treated group.

pH change (Fig. 2e, Fig. S4). As in the previous ThT assay, ANA was incubated in several pH solvents and was confirmed to have Aβ plaque disaggregation efficacy at all pH levels. In particular, ANA had the highest Aβ plaque disaggregation efficacy between pH 5 and 7.4, and the pH around the Aβ plaque was between pH 6 and pH 7.4. This substantiates that ANA holds promising potential for clinical applications.

Next, the disaggregation of Aβ plaque after treatment of ANA was verified by transmission electron microscopy (TEM) imaging (Fig. 2f) and confocal laser scanning microscope (CLSM) imaging (Fig. 2g and 2h, Fig. S5). TEM and CLSM data were acquired from two sets; (i) Aβ plaque (20 μM) and (ii) ANA (100 μM)-treated Aβ plaque (20 μM). The TEM images represented that Aβ plaque was significantly disaggregated in the ANA-treated set. For the CLSM imaging, thioflavin S (ThS) was treated to the Aβ plaque before adding ANA. As shown in Fig. 2g, a significantly reduced fluorescence intensity of ThS was observed in the ANA-treated set, which confirms that Aβ plaque disaggregation induced an emission intensity loss of ThS. The emission intensity plots of ThS fluorescence images (Fig. 2h) corresponds with the TEM and CLSM imaging results.

3.2. Preparation and characterization of Biotin-$CaCl_2$-ANA-pSiNPs (BCAP)

The in vitro Aβ plaque disaggregation screening (step 1) confirmed ANA as a hit compound for further study. However, as described above, the drawbacks of such negatively charged bioactive molecules require a nano-carrier to deliver itself to the brain selectively with high BBB penetration. Among the various nano-carrier, porous silicon nanoparticles (pSiNPs) have been shown high loading efficacy, low cytotoxicity, non-toxic dissolution products, and high tissue specificity, which can even deliver drugs to the brain across the BBB, through surface modification [49,50].

The pSiNPs were prepared by electrochemical etching of a single crystal silicon wafer under a perforating etching condition and ultrasonic frustration within DI H_2O (see details in the Experimental section) [51]. As-prepared pSiNPs were vortexed with ANA in the presence of $CaCl_2$ for the calcium-silicate surface coating and the ANA loading within the pore structure of pSiNPs. The resulting intermediate, named CAP, was further functionalized with biotin-PEG-Si$(OEt)_3$ (5000 Da) by

hydrolytic condensation (Fig. 3a). The resulting nano-platform was named BCAP (Biotin-$CaCl_2$-ANA-pSiNPs), which is expected to be accumulated to the AD brain by targeting biotin receptors in the endothelial cells of the AD blood-brain barrier (BBB). BCAP had a loading efficiency of ANA at around 44.75%. The loading efficiency of ANA was determined by the following equation (1). To check the loading efficiency, UV/vis absorption and emission spectra of ANA were first measured (Fig. S6). ANA showed a maximum absorption wavelength at 338 nm with a maximum emission intensity at 420 nm, and the amount of ANA loaded was confirmed by measuring the emission intensity changes according to the concentration of ANA (Fig. S7).

$$\text{Loading efficiency}\ (\%) = \frac{W_{\text{total}}\ \text{ANA} - W_{\text{un-loaded}}\ \text{ANA}}{W_{\text{total}}\ \text{ANA} + W_{\text{total}}\ \text{NPs}} \times 100 \qquad \text{eq.(1)}$$

As-prepared pSiNP displayed a homogeneous particle size (mean hydrodynamic diameter of 141.1 nm, polydispersity index; PDI: 0.183, Fig. 3b) and a negative zeta-potential value of -22.8 ± 7.13 mV (Fig. 3c) measured by dynamic light scattering (DLS). The ANA-loaded pSiNPs (CAP) showed a slightly increased size of around 179.3 nm (PDI: 0.192) with a slightly reduced negative surface charge (-12.1 ± 4.84 mV). The PEGylated nanoparticle, BCAP, showed a slight size increment to 201.4 nm (PDI: 0.106) with an increased negative surface charge (-29.4 ± 6.48 mV). After confirming the size and surface charge of nanoparticles, the attenuated total reflectance Fourier-transform infrared spectrum (ATR-FTIR) analysis was conducted to confirm that the ANA loading and PEG surface functionalization were properly performed (Fig. 3d, Fig. S8). The ATR-FTIR of the pristine pSiNPs displayed two characteristic bands corresponding to ν(O–H) stretching at 3550–3200 cm^{-1} and ν(Si–O) stretching at 1065 cm^{-1} [52]. The CAP showed several bands including bands corresponding to ν(N–H) at 3439 cm^{-1} and ν(C=C) at 1562 cm^{-1} that were also observed in ANA [53,54]. BCAP also showed several fingerprint bands including bands corresponding to ν(C–H) at 2921–2882 cm^{-1} and ν(C–O) at 1084 cm^{-1} that was also observed in biotin-PEG [55]. These ATR-FTIR results demonstrated that ANA was loaded within the pSiNPs, and biotin-PEG was successfully PEGylated on the surface. In addition, the morphology changes of nanoparticles were checked using TEM imaging (Fig. 3e). The pore size obtained from each TEM image was 11.1 nm for pSiNPs, 9.3 nm for ANA-pSiNPs, 3.9 nm for CAP, and 2.8 nm for BCAP (Fig. S9). The results confirmed that the pore of CAP and BCAP was clogged due to the calcium-silicate coating, but the ANA-pSiNPs ($CaCl_2$ non-treated set) showed an open-pore structure that is prone to leak ANA.

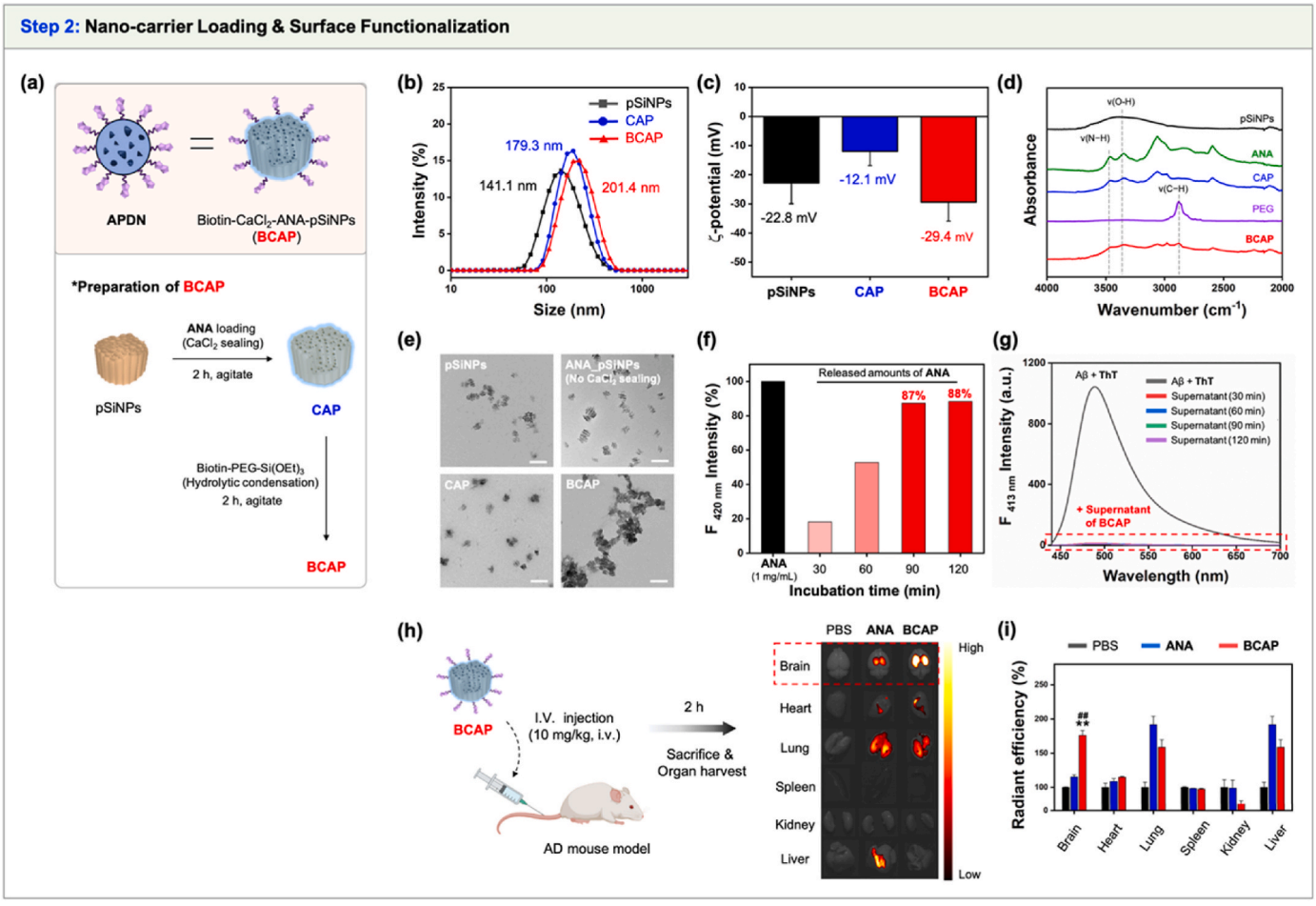

Fig. 3. (a) Schematic illustration of the preparation of BCAP. CAP: ANA-loaded and calcium-silicate-sealed pSiNPs. BCAP: Biotin-functionalized CAP. Silane-PEG-biotin (5000 Da) was used. (b) Average hydrodynamic diameter and (c) zeta-potential value of nano-formulations analyzed by dynamic light scattering (DLS). Polydispersity index: <0.3. (d) Attenuated total reflectance Fourier transform infrared (ATR-FTIR) spectra of nano-formulations, ANA, and Silane PEG Biotin. Symbols: ν = stretching. (e) Transmission electron microscopy (TEM) images of pSiNPs, ANA-pSiNPs (no $CaCl_2$ sealing), CAP, and BCAP. Scale bar: 100 nm. (f) Emission intensity plot (at 420 nm) of ANA accumulated from the supernatant of BCAP (1 mg) during incubation (interval time: 30–120 min). Excitation wavelength: 338 nm. (g) Emission spectra of ThT (10 μM) in the presence of Aβ plaque (10 μM) and the supernatant (ANA-containing) of BCAP (PBS buffer, pH 7.4, at 25 °C) that were obtained at each incubation time point. Excitation wavelength: 413 nm. (h) Scheme illustration of the animal study and FTIS image of AD mouse model organs. (i) The radiant efficiency plot of each organ from the FTIS image. The images were acquired tracking the signals of ANA (Channel: 390–490 nm excitation, 500–550 nm detection channel). The data are shown as the means ± S.E.M. (n = 4). **<0.01 when compared to the PBS group. ##<0.01 when compared to the ANA group.

Next, the release profile of ANA from BCAP and its Aβ plaque disaggregation ability (Fig. 3f and 3g). BCAP (1 mg) was dissolved in PBS (pH 7.4) and vortexed in a shaking incubator at 37 °C. The supernatants were collected every 30 min, and their UV/vis absorption and emission spectra were measured (Fig. 3f, Fig. S10). The spectra showed that almost all of ANA were released from BCAP within 90 min. The Aβ plaque disaggregating ability of ANA within the supernatant was confirmed by ThT assay in the presence of Aβ plaques (10 μM) (Fig. 3g, Fig. S11). As ANA existed within the supernatant, most of the Aβ plaques were disaggregated after treatment of the supernatant at all time points. Such results proved that the properties of ANA were maintained even after its loading/releasing from the nano-formulations. After confirming the basic characterization of nano-formulation, an animal study was conducted to confirm the AD brain targeting ability of BCAP. BCAP (10 mg/kg) was administered via tail vein (intravenous, i.v.) to balb/c mice (AD mouse model). An AD mouse model was prepared by administering Aβ plaque via intracerebroventricular (i.c.v.) injection. After administration and 2 h of blood circulation of BCAP, the main organs (brain, heart, lung, spleen, kidney, and liver) were harvested from all mice and their fluorescence signals were analyzed (Fig. 3h). The fluorescence signals of ANA were tracked to monitor the distribution of BCAP in the body using the imaging procedures, and the radiant efficiency of fluorescence from each image was analyzed (Fig. 3i). Significantly high radiant efficiency was observed in the brain of the BCAP-treated group compared to other groups, which denotes that a greater amount of BCAP was accumulated to the AD brain and BCAP has superior brain-targeting ability in the AD mouse model. The high fluorescence intensity in the lung or liver suggested that some ANA were distributed in the alveolar-capillary barrier of the lung since the drugs were injected intravenously [56]. In addition, since the drug still remained in the liver, it could be confirmed that the drug metabolism had not fully progressed and that the drug metabolism in the lungs rich in capillaries was progressing slowly accordingly [57,58].

3.3. Therapeutic efficacy analysis of BCAP

We confirmed that ANA and its nano-formulation, BCAP, could disaggregate the Aβ plaque efficiently under in vitro conditions. In order

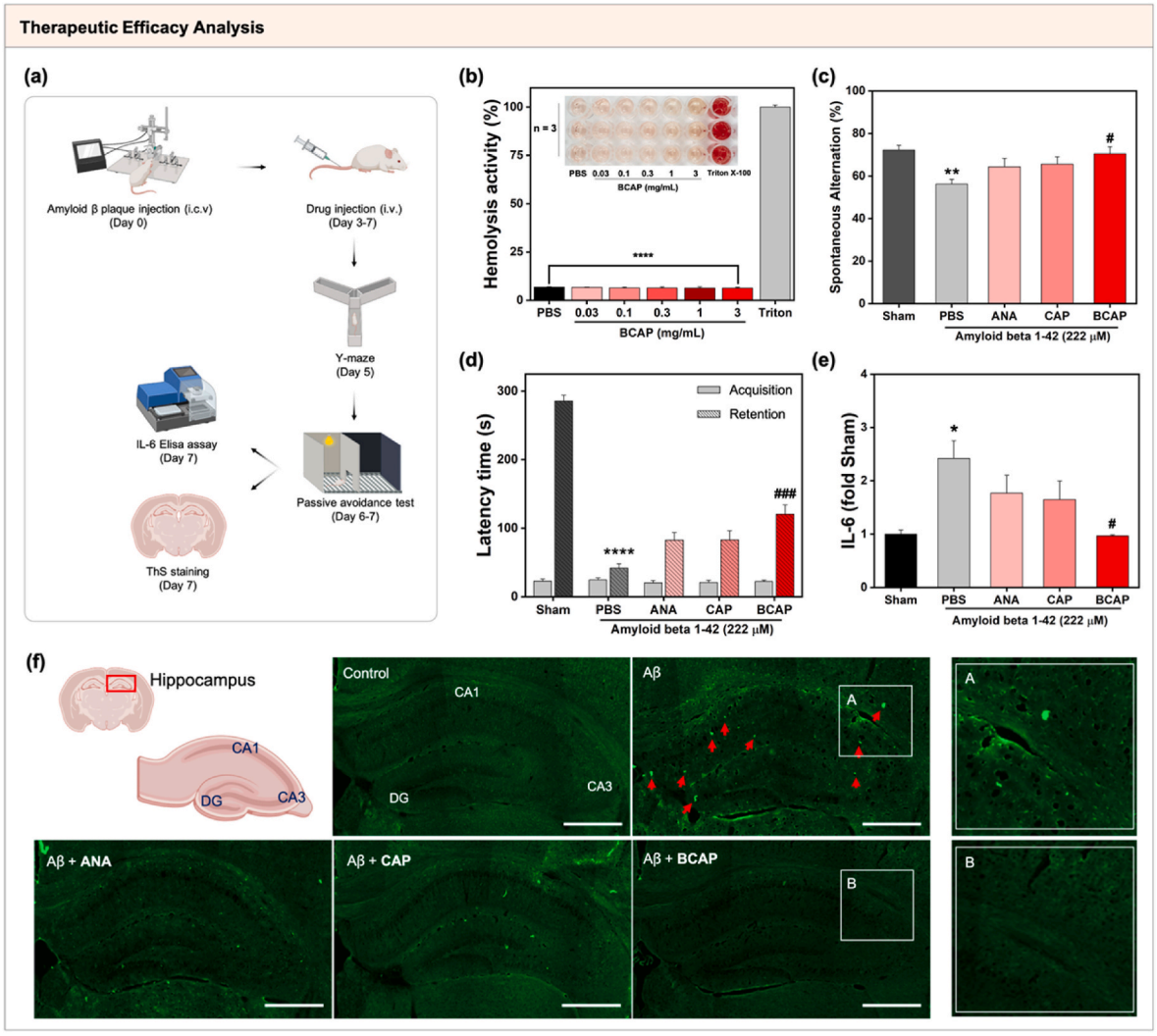

Fig. 4. (a) Schematic diagram of the animal study. AD mouse model was prepared by stereotaxic administration of Aβ plaque. Drug injection (i.v.) was conducted from day 3–7. Main test: Y-maze test, passive avoidance test (PAT), IL-6 ELISA assay, and ThS staining of brain slice. (b) Hemolysis analysis results of BCAP. The data are shown as the means ± S.E.M. (n = 3). ****<0.0001 when compared to the Triton X-100 group. (c) Spontaneous alternation results of the Y-maze test. The data are shown as the means ± S.E.M. (n = 8). **<0.01 when compared to the sham group. #<0.05 when compared to the PBS group. (d) The results of PAT. The data are shown as the means ± S.E.M. (n = 8). ****<0.0001 when compared to the sham group. ###<0.001 when compared to the PBS group. (e) ELISA assay of interleukin 6 (IL-6). The data are shown as the means ± S.E.M. (n = 4). *<0.05 when compared to the sham group. #<0.05 when compared to the PBS group. (f) Fluorescence image of hippocampal slices stained with ThS. The hippocampal slices were harvested from 5 groups (red arrows: location Aβ plaques).

to verify the in vivo activity of ANA and BCAP, behavioral tests, interleukin 6 (IL-6) level analysis, and brain tissue staining were conducted in the AD mouse model (Fig. 4a). For the behavioral tests, the Y-maze test and passive avoidance test (PAT) were carried out to see whether ANA and BCAP can actually disaggregate Aβ plaques in vivo and improve the memory deficit. IL-6 is a representative cytokine that could be up-regulated by Aβ plaques and is a biomarker to track the level of Aβ plaques in the brain. The ThS staining was introduced to visualize the Aβ plaque's distribution in the brain, particularly with a focus on the hippocampus in the imaging analysis. Before proceeding the in vivo experiment, the applicable working concentrations of ANA and BCAP were determined through hemolysis assay (Fig. 4b, Fig. S12). The hemolysis assay results of ANA and BCAP showed almost no toxicity up to a concentration of 3 mg/mL for both substances, which represented a high bioavailability. Based on the hemolysis assay results, the in vivo administration concentration was set to 8 mg/kg for the animal study.

The AD mouse model was randomly divided into four groups; (i) PBS-treated group, (ii) ANA-treated group, (iii) CAP-treated group, and (iv) BCAP-treated group. The sham group (no Aβ plaques injection) was used as a control to confirm whether the Aβ plaques were properly formed within the AD mouse model brain. Each formulation was treated to the AD mouse model (Aβ plaque injection) every day from Day 3 to Day 7. On Day 5, the Y-maze test was performed to measure the working memory and spatial memory. The Y-maze test results demonstrated the percentage of spontaneous alternation and the number of total arm entries. The percentage of spontaneous alternation is a result of the spatial working memory of the mice, and this value is high if the memory of the mouse is normal. The number of total arm entries indicates how actively the mice moved, which can be changed by drugs or other factors. The results of spontaneous alternation obtained based on similar activity levels were used as reliable data. The results of the Y-maze test indicated that the spontaneous alternation level of the PBS-treated group was significantly lower compared to the normal group (sham group), but the BCAP-treated group maintained almost the same level (Fig. 4c). The results demonstrate that BCAP is effective in the AD brain, and the AD mouse model was properly prepared following the preparation methods in this work. However, there were no significant differences in the total arm entries of mice in all groups (Fig. S13).

Next, the passive avoidance test (PAT) was performed on Days 6–7 to measure traumatic memory recovery of the AD brain by comparing the latency time of mice in the given experimental condition. PAT can provide acquisition results from the mice on the first day and the retention results that confirmed memory retention by the mice on the second day. Retention results obtained based on similar acquisition results are used as reliable results. In the acquisition results, as in the total arm entry results of the Y-maze test, there was no significant difference among all groups, so we assumed that the PAT memory test was not affected by hyperactivity of the Aβ plaque or treatment of ANA/nano-formulations. On the other hand, there was a clear difference between the groups in the retention results. In the PBS-treated group, the latency time of the AD mice was significantly shorter when compared with the sham group. The latency time was slightly longer in the ANA-/CAP-treated group and significantly increased in the BCAP-treated group (Fig. 4d). The results of the Y-maze test and the PAT represent that BCAP had a high efficacy of memory improvement for the AD mice.

After confirming the memory improvement by BCAP, the (i) IL-6 level analysis and (ii) fluorescence-based Aβ plaque staining were conducted to confirm that this memory improvement was caused by disaggregation of Aβ plaques. Firstly, the change in the level of IL-6 was analyzed (Fig. 4e). IL-6 is a multifunctional cytokine that regulates immune response, hematopoiesis, acute phase response, and inflammation. Several previous reports reported that IL-6 is the most representative cytokine that is affected by Aβ plaque. The level of IL-6 was confirmed by ELISA assay by only separating plasma from the mice blood of each group on Day 7 when the behavioral experiment was finished. It was confirmed that the level of IL-6 in the PBS-treated group increased about 2.5 times compared to the sham group, but the level of IL-6 decreased in the group treated with ANA, CAP, and BCAP, with the most significant decrement in the BCAP-treated group. These results indicate that the inflammatory response of mice was increased by Aβ plaques, which could be reduced by BCAP that disaggregates Aβ plaques. Secondly, ThS staining was performed on the hippocampus of all groups of mice (Fig. 4f). In the hippocampus slice image of the AD mice, a bright fluorescence signal of ThS was observed at the spot of Aβ plaques. However, the spots were partially reduced in the ANA-/CAP-treated group, and almost no spots were observed in the BCAP-treated group. The results of these in vivo experiments indicate that ANA has clear Aβ plaque disaggregation efficacy even in vivo, and its nano-formulation (BCAP) specifically delivers ANA to the AD brain.

4. Conclusion

In this study, we disclosed a new bioactive molecule, ANA, that disaggregates Aβ plaque efficiently and its delivery system to the AD brain using pSiNPs. Our rationale basis is that the sulfonic acid could be a key moiety to find a new therapeutic agent for AD, and a hit compound was discovered as a result of the agent library screening. The newly discovered ANA showed superior activity for the Aβ plaque disaggregation with high biocompatibility. We introduced a nanoparticle-based formulation of ANA as a potential AD therapeutic nano-platform by delivering large amounts of ANA through the blood-brain barrier (BBB) with high brain accumulation. The nano-platform, called BCAP, was prepared based on ANA-loaded and calcium-silicate-coated pSiNPs with biotin-PEG functionalization on the surface. BCAP disaggregated Aβ plaques with a high efficacy in vitro and with a high biocompatibility in vivo, which ameliorated memory impairment and reduced the level of inflammation that were verified by the decrease of the actual amount of Aβ plaque in the AD brain. We believe that ANA can be developed as a new therapeutic candidate for the treatment of AD, and its nano-formulation, BCAP, can open a new era for more precise AD treatment.

Ethics approval and consent to participate

Studies involving human participants: None.

Studies involving animals: Animal treatment and maintenance were performed according to the Animal Care and Use Guidelines by Kyung Hee University. All experimental protocols were approved by the Institutional Animal Care and Use Committee of Kyung Hee University (Approval number: KHSASP-22-024).

CRediT authorship contribution statement

Jaehoon Kim: Conceptualization, Methodology, Validation, Formal analysis, Investigation, Data curation, Writing – original draft, Writing – review & editing, Visualization. **Hyeji Um:** Methodology, Formal analysis, Writing – original draft. **Na Hee Kim:** Methodology, All authors have read and agreed with the published version of the manuscript. **Dokyoung Kim:** Conceptualization, Writing – original draft, Writing – review & editing, Visualization, Supervision, Project administration, Data curation.

Declaration of competing interest

The authors declare the following competing financial interest(s): The authors are listed as inventors on a pending patent application related to the technology described in this work.

Acknowledgments

This research was supported by Basic Science Research Program through the National Research Foundation (NRF) of Korea funded by the Ministry of Education (2018-R1A6A1A03025124; D.K.). This research

was supported by Bio & Medical Technology Development Program of the NRF of Korea funded by the Ministry of Science & ICT (2022-M3A9H1014157, 2021-M3A9I5030523; D.K.) and a grant from Korea Health Technology R&D Project of the Korea Health Industry Development Institute (KHIDI) funded by the Ministry of Health & Welfare, Republic of Korea (HI21C0239; D.K.). This work was supported by the National Research Foundation of Korea (NRF) grant funded by the Korea government (MSIT) (2022-R1F1A1069954; D.K.).

Appendix A. Supplementary data

Supplementary data to this article can be found online at https://doi.org/10.1016/j.bioactmat.2023.01.006.

References

[1] Y. Hou, X. Dan, M. Babbar, Y. Wei, S.G. Hasselbalch, D.L. Croteau, V.A. Bohr, Ageing as a risk factor for neurodegenerative disease, Nat. Rev. Neurol. 15 (10) (2019) 565–581.
[2] G.B. Frisoni, D. Altomare, D.R. Thal, F. Ribaldi, R. van der Kant, R. Ossenkoppele, K. Blennow, J. Cummings, C. van Duijn, P.M. Nilsson, The probabilistic model of Alzheimer disease: the amyloid hypothesis revised, Nat. Rev. Neurosci. 23 (1) (2022) 53–66.
[3] D. Aarsland, L. Batzu, G.M. Halliday, G.J. Geurtsen, C. Ballard, K. Ray Chaudhuri, D. Weintraub, Parkinson disease-associated cognitive impairment, Nat. Rev. Dis. Prim. 7 (1) (2021) 1–21.
[4] F.O. Walker, Huntington's disease, Lancet 369 (9557) (2007) 218–228.
[5] A. Alzheimer, Uber eine eigenartige Erkrankung der Hirnrinde, Zentralbl. Nervenh. Psych. 18 (1907) 177–179.
[6] M.G. Savelieff, G. Nam, J. Kang, H.J. Lee, M. Lee, M.H. Lim, Development of multifunctional molecules as potential therapeutic candidates for Alzheimer's disease, Parkinson's disease, and amyotrophic lateral sclerosis in the last decade, Chem. Rev. 119 (2) (2018) 1221–1322.
[7] M. Goedert, M.G. Spillantini, A century of Alzheimer's disease, Science 314 (5800) (2006) 777–781.
[8] C.M. Henstridge, B.T. Hyman, T.L. Spires-Jones, Beyond the neuron–cellular interactions early in Alzheimer disease pathogenesis, Nat. Rev. Neurosci. 20 (2) (2019) 94–108.
[9] J. Zhou, P. Jangili, S. Son, M.S. Ji, M. Won, J.S. Kim, Fluorescent diagnostic probes in neurodegenerative diseases, Adv. Mater. Lett. 32 (51) (2020), 2001945.
[10] M. Vaz, S. Silvestre, Alzheimer's disease: recent treatment strategies, Eur. J. Pharmacol. 887 (2020), 173554.
[11] J.M. Long, D.M. Holtzman, Alzheimer disease: an update on pathobiology and treatment strategies, Cell 179 (2) (2019) 312–339.
[12] J.A. Hardy, G.A. Higgins, Alzheimer's disease: the amyloid cascade hypothesis, Science 256 (5054) (1992) 184–185.
[13] H. Choi, E. Kim, J.Y. Choi, E. Park, H.J. Lee, Potent therapeutic targets for treatment of Alzheimer's disease: amyloid degrading enzymes, Bull. Korean Chem. Soc. 42 (11) (2021) 1419–1429.
[14] P.-P. Liu, Y. Xie, X.-Y. Meng, J.-S. Kang, History and progress of hypotheses and clinical trials for Alzheimer's disease, Signal Transduct. Target. Ther. 4 (1) (2019) 1–22.
[15] H. Hampel, J. Hardy, K. Blennow, C. Chen, G. Perry, S.H. Kim, V.L. Villemagne, P. Aisen, M. Vendruscolo, T. Iwatsubo, The amyloid-β pathway in Alzheimer's disease, Mol. Psychiatry 26 (10) (2021) 5481–5503.
[16] H. Ashrafian, E.H. Zadeh, R.H. Khan, Review on Alzheimer's disease: inhibition of amyloid beta and tau tangle formation, Int. J. Biol. Macromol. 167 (2021) 382–394.
[17] J. Sevigny, P. Chiao, T. Bussière, P.H. Weinreb, L. Williams, M. Maier, R. Dunstan, S. Salloway, T. Chen, Y. Ling, The antibody aducanumab reduces Aβ plaques in Alzheimer's disease, Nature 537 (7618) (2016) 50–56.
[18] H. Hampel, R. Vassar, B. De Strooper, J. Hardy, M. Willem, N. Singh, J. Zhou, R. Yan, E. Vanmechelen, A. De Vos, The β-secretase BACE1 in Alzheimer's disease, Biol. Psychiatry 89 (8) (2021) 745–756.
[19] C.H. Van Dyck, Anti-amyloid-β monoclonal antibodies for Alzheimer's disease: pitfalls and promise, Biol. Psychiatry 83 (4) (2018) 311–319.
[20] K. Rajasekhar, M. Chakrabarti, T. Govindaraju, Function and toxicity of amyloid beta and recent therapeutic interventions targeting amyloid beta in Alzheimer's disease, Chem. Commun. 51 (70) (2015) 13434–13450.
[21] K. Rajasekhar, T. Govindaraju, Current progress, challenges and future prospects of diagnostic and therapeutic interventions in Alzheimer's disease, RSC Adv 8 (42) (2018) 23780–23804.
[22] S. Maher, T. Kumeria, Y. Wang, G. Kaur, D. Fathalla, G. Fetih, A. Santos, F. Habib, A. Evdokiou, D. Losic, From the mine to cancer therapy: natural and biodegradable theranostic silicon nanocarriers from diatoms for sustained delivery of chemotherapeutics, Adv. Healthc. Mater. 5 (20) (2016) 2667–2678.
[23] S.J. McInnes, A. Santos, T. Kumeria, Porous Silicon Particles for Cancer Therapy and Bioimaging, Nanooncology, Springer, 2018, pp. 305–340.
[24] H.A. Santos, J. Riikonen, J. Salonen, E. Mäkilä, T. Heikkilä, T. Laaksonen, L. Peltonen, V.-P. Lehto, J. Hirvonen, In vitro cytotoxicity of porous silicon microparticles: effect of the particle concentration, surface chemistry and size, Acta Biomater 6 (7) (2010) 2721–2731.
[25] S.J. Vannucci, F. Maher, I.A. Simpson, Glucose transporter proteins in brain: delivery of glucose to neurons and glia, Glia 21 (1) (1997) 2–21.
[26] C. Zhang, J. Chen, C. Feng, X. Shao, Q. Liu, Q. Zhang, Z. Pang, X. Jiang, Intranasal nanoparticles of basic fibroblast growth factor for brain delivery to treat Alzheimer's disease, Int. J. Pharm. 461 (1–2) (2014) 192–202.
[27] S. Wohlfart, S. Gelperina, J. Kreuter, Transport of drugs across the blood–brain barrier by nanoparticles, J. Control. Release 161 (2) (2012) 264–273.
[28] L. Ordóñez-Gutiérrez, F. Re, E. Bereczki, E. Ioja, M. Gregori, A.J. Andersen, M. Antón, S.M. Moghimi, J.-J. Pei, M. Masserini, Repeated intraperitoneal injections of liposomes containing phosphatidic acid and cardiolipin reduce amyloid-β levels in APP/PS1 transgenic mice, Nanomedicine 11 (2) (2015) 421–430.
[29] R.G. Pinheiro, A.J. Coutinho, M. Pinheiro, A.R. Neves, Nanoparticles for targeted brain drug delivery: what do we know? Int. J. Mol. Sci. 22 (21) (2021), 11654.
[30] H. Wang, J. Pevsner, Detection of endogenous biotin in various tissues: novel functions in the hippocampus and implications for its use in avidin-biotin technology, Cell Tissue Res 296 (3) (1999) 511–516.
[31] R. Spector, D. Mock, Biotin transport through the blood-brain barrier, J. Neurochem. 48 (2) (1987) 400–404.
[32] B. Baur, E.R. Baumgartner, Biotin and biocytin uptake into cultured primary calf brain microvessel endothelial cells of the blood–brain barrier, Brain Res 858 (2) (2000) 348–355.
[33] B. Purushothaman, J. Lee, S. Hong, J.M. Song, Multifunctional TPP-PEG-biotin self-assembled nanoparticle drug delivery-based combination therapeutic approach for co-targeting of GRP78 and lysosome, J. Nanobiotechnology 18 (1) (2020) 1–19.
[34] J. Kim, D. Kim, 4-(2-Hydroxyethyl)-1-piperazine ethane sulfonic acid repositioning: amyloid disaggregating agent and its sustained-release system, Bull. Korean Chem. Soc. 43 (1) (2022) 78–82.
[35] H.Y. Kim, H.V. Kim, S. Jo, C.J. Lee, S.Y. Choi, D.J. Kim, Y. Kim, EPPS rescues hippocampus-dependent cognitive deficits in APP/PS1 mice by disaggregation of amyloid-β oligomers and plaques, Nat. Commun. 6 (1) (2015) 1–14.
[36] N.D. Younan, J.H. Viles, A comparison of three fluorophores for the detection of amyloid fibers and prefibrillar oligomeric assemblies. ThT (thioflavin T); ANS (1-anilinonaphthalene-8-sulfonic acid); and bisANS (4, 4′-dianilino-1, 1′-binaphthyl-5, 5′-disulfonic acid), Biochemistry 54 (28) (2015) 4297–4306.
[37] A.D. Ferrão-Gonzales, B.K. Robbs, V.H. Moreau, A.l. Ferreira, L. Juliano, A. P. Valente, F.C. Almeida, J.L. Silva, D. Foguel, Controlling β-amyloid oligomerization by the use of naphthalene sulfonates: trapping low molecular weight oligomeric species, J. Biol. Chem. 280 (41) (2005) 34747–34754.
[38] B. Bolognesi, J.R. Kumita, T.P. Barros, E.K. Esbjorner, L.M. Luheshi, D.C. Crowther, M.R. Wilson, C.M. Dobson, G. Favrin, J.J. Yerbury, ANS binding reveals common features of cytotoxic amyloid species, ACS Chem. Biol. 5 (8) (2010) 735–740.
[39] J. Kealy, C. Greene, M. Campbell, Blood-brain barrier regulation in psychiatric disorders, Neurosci. Lett. 726 (2020), 133664.
[40] V. Ceña, P. Játiva, Nanoparticle crossing of blood–brain barrier: a road to new therapeutic approaches to central nervous system diseases, Future Medicine (2018) 1513–1516.
[41] N.M. Lyra e Silva, R.A. Gonçalves, T.A. Pascoal, R.A. Lima-Filho, E.d.P.F. Resende, E.L. Vieira, A.L. Teixeira, L.C. de Souza, J.A. Peny, J.T. Fortuna, Pro-inflammatory interleukin-6 signaling links cognitive impairments and peripheral metabolic alterations in Alzheimer's disease, Transl. Psychiatry 11 (1) (2021) 1–15.
[42] H. Lin, S.G. Dixon, W. Hu, E.D. Hamlett, J. Jin, A. Ergul, G.Y. Wang, p38 MAPK is a major regulator of amyloid beta-induced IL-6 expression in human Microglia, Mol. Neurobiol. 59 (9) (2022) 5284–5298.
[43] A.D. Snow, J.A. Cummings, R.E. Tanzi, T. Lake, In vitro comparison of major memory-support dietary supplements for their effectiveness in reduction/inhibition of beta-amyloid protein fibrils and tau protein tangles: key primary targets for memory loss, Sci. Rep. 11 (1) (2021) 1–23.
[44] D. Kim, S.H. Baik, S. Kang, S.W. Cho, J. Bae, M.-Y. Cha, M.J. Sailor, I. Mook-Jung, K.H. Ahn, Close correlation of monoamine oxidase activity with progress of Alzheimer's disease in mice, observed by in vivo two-photon imaging, ACS Cent. Sci. 2 (12) (2016) 967–975.
[45] T.S. Choi, H.J. Lee, J.Y. Han, M.H. Lim, H.I. Kim, Molecular insights into human serum albumin as a receptor of amyloid-β in the extracellular region, J. Am. Chem. Soc. 139 (43) (2017) 15437–15445.
[46] H.Y. Kim, D.K. Lee, B.-R. Chung, H.V. Kim, Y. Kim, Intracerebroventricular injection of amyloid-β peptides in normal mice to acutely induce Alzheimer-like cognitive deficits, J. Vis. Exp. 109 (2016), e53308.
[47] H.J. Bae, J. Kim, S.J. Jeon, J. Kim, N. Goo, Y. Jeong, K. Cho, M. Cai, S.Y. Jung, K. J. Kwon, Green tea extract containing enhanced levels of epimerized catechins attenuates scopolamine-induced memory impairment in mice, J. Ethnopharmacol. 258 (2020), 112923.
[48] J. Kim, Y.H. Seo, J. Kim, N. Goo, Y. Jeong, H.J. Bae, S.Y. Jung, J. Lee, J.H. Ryu, Casticin ameliorates scopolamine-induced cognitive dysfunction in mice, J. Ethnopharmacol. 259 (2020), 112843.
[49] M. Luo, G. Lewik, J.C. Ratcliffe, C.H.J. Choi, E. Mäkilä, W.Y. Tong, N.H. Voelcker, Systematic evaluation of transferrin-modified porous silicon nanoparticles for targeted delivery of doxorubicin to glioblastoma, ACS Appl. Mater. Interfaces 11 (37) (2019) 33637–33649.
[50] V. Balasubramanian, A. Domanskyi, J.-M. Renko, M. Sarparanta, C.-F. Wang, A. Correia, E. Mäkilä, O.S. Alanen, J. Salonen, A.J. Airaksinen, Engineered antibody-functionalized porous silicon nanoparticles for therapeutic targeting of pro-survival pathway in endogenous neuroblasts after stroke, Biomaterials 227 (2020), 119556.

[51] J.-H. Park, L. Gu, G. Von Maltzahn, E. Ruoslahti, S.N. Bhatia, M.J. Sailor, Biodegradable luminescent porous silicon nanoparticles for in vivo applications, Nat. Mater. 8 (4) (2009) 331–336.
[52] A. Bertucci, K.-H. Kim, J. Kang, J.M. Zuidema, S.H. Lee, E.J. Kwon, D. Kim, S. B. Howell, F. Ricci, E. Ruoslahti, Tumor-targeting, microRNA-silencing porous silicon nanoparticles for ovarian cancer therapy, ACS Appl. Mater. Interfaces 11 (27) (2019) 23926–23937.
[53] H.A. Alhazmi, FT-IR spectroscopy for the identification of binding sites and measurements of the binding interactions of important metal ions with bovine serum albumin, Sci. Pharm. 87 (1) (2019) 5.
[54] K. Gipson, K. Stevens, P. Brown, J. Ballato, Infrared spectroscopic characterization of photoluminescent polymer nanocomposites, J. Appl. Spectrosc. 2015 (2015).
[55] A. Krüger, A. Bürkle, A. Mangerich, K. Hauser, A combined approach of surface passivation and specific immobilization to study biomolecules by ATR-FTIR spectroscopy, Biomed. Spectrosc. Imaging 7 (1–2) (2018) 25–33.
[56] M.I. Hermanns, J. Kasper, P. Dubruel, C. Pohl, C. Uboldi, V. Vermeersch, S. Fuchs, R.E. Unger, C.J. Kirkpatrick, An impaired alveolar-capillary barrier in vitro: effect of proinflammatory cytokines and consequences on nanocarrier interaction, J. R. Soc. Interface (2010) S41–S54.
[57] O.A. Almazroo, M.K. Miah, R. Venkataramanan, Drug metabolism in the liver, Clin. Liver Dis. 21 (1) (2017) 1–20.
[58] H. Remmer, The role of the liver in drug metabolism, Am. J. Med 49 (5) (1970) 617–629.